

Electrodeposition of Ni, Fe and Ni-Fe Alloys in Two Ionic Liquids: (tri (n-butyl) [2-methoxy-2-oxoethyl] Ammonium bis (trifluoromethylsulfonyl) [BuGBOEt] [Tf₂N]) and (1-butyl-1-methylpyrrolidinium bis trifluoromethylsulfonyl) imide ([P_{1,4}] [Tf₂N])

Rafik Maizi^{1,*}, Patrick Fricoteaux², Aminou Mohamadou³, Athmane Meddour¹, Céline Rousse^{3,*}

¹ Laboratoire de physique des matériaux L2PM, Université du 8 mai 1945 Guelma, B.P 401, 24000 Guelma, Algérie.

² LISM EA 4695, UFR Sciences Exactes et Naturelles, B.P.1039, 51687 Reims Cedex 02, France.

³ ICMR UMR CNRS 7312, UFR Sciences Exactes et Naturelles, B.P.1039, 51687 Reims Cedex 02, France.

*E-mail: rmaizi24@gmail.com celine.rousse@univ-reims.fr

Received: 23 April 2016 / Accepted: 21 June 2016 / Published: 7 July 2016

Ni, Fe and Ni-Fe alloys electrodeposition were tested in two ionic liquids. The first one is a commercial (1-butyl-1-methylpyrrolidinium bis(trifluoromethylsulfonyl)imide ([P_{1,4}][Tf₂N])) and the second is a homemade (tri(n-butyl)[2-ethoxy-2oxoethyl]ammonium bis (trifluoromethylsulfonyl)imide([BuGBOEt][Tf₂N])). Covering iron deposits was obtained in the [BuGBOEt][Tf₂N]. Nickel deposition was only possible in the [P_{1,4}][Tf₂N]. Ni-Fe alloys were obtained from the [P_{1,4}][Tf₂N] solvent. The study of the evolution of alloys composition versus polarisation shows irregular evolution depending on the applied potential. The alloys composition varies approximately between Ni₇₀-Fe₃₀ and Ni₉₀-Fe₁₀ for applied potentials including to - 1.8 V and - 4 V versus Ni electrode. The chemical composition, the surface morphology and the structure, of deposits were characterized by scanning electron microscopy (SEM), energy dispersive analysis (EDX) and X-ray diffraction (XRD).

Keywords: Fe; Ni; Ni-Fe alloys; Electrodeposition; Ionic liquids

1. INTRODUCTION

Due to their unique physical properties, Fe, Ni and Ni-Fe alloys have been intensively investigated during the last decades.

Preparation of these materials by electrodeposition technique allows a production at low fabrication costs, with great purity and large choice of the piece shapes. Many studies have reported on anomalous compartment of Ni-Fe alloys [1], and many investigations have been carrying out on the influence of electrodeposition conditions, such as: electrolyte composition, pH, polarization, convection, magnetic field superimposition, additional agents...[2-12].

It is noted that, the nickel or the iron electrodeposition in aqueous solution leads to low current efficiency. The hydrogen evolution reaction occurs in the course of electrodeposition resulting in profound effect on current efficiency and quality of deposits (hydrogen embrittlement).

Room-temperature ionic liquids (RTILs) are expected to be a good alternative aprotic media for electrodeposition of various metals. At the beginning, the use of these solvents concerned essentially materials which cannot be electroplated from aqueous solutions [13-15]. But, some other advantages are also interesting: inflammability, negligible vapor pressure, absence of hydrogen evolution simultaneously with a metal deposition, refinement of the grain size.

The electrodeposition of Ni and its alloys has been mainly studied in chloroaluminate based solvent, named first generation RTILs [16-19]. But the high sensitivity of aluminum chloride towards oxygen and moisture as delayed progress in their practical applications [20-22]. Therefore, a second generation of RTILs (air and water-stable RTILs) has been developed. The most popular water-stable RTILs are those containing anions such as tetrafluoroborate (BF_4^-), hexafluorophosphate (PF_6^-) or bis(trifluoromethylsulfonyl)imide (Tf_2N^-) [23-24]. The bis(trifluoromethylsulfonyl)imide (Tf_2N^-) based ionic liquids are expected to be preferable for electrodeposition of various metals, including Ni, since these ionic liquids are stable against moisture and immiscible with water. Zhu et al. [25-26] studied the effect of additives, such as acetone, thiourea or acetonitrile, on the electrodeposition of Ni from the 1-butyl-1-methylpyrrolidinium bis(trifluoromethylsulfonyl)amide ($[\text{P}_{1,4}][\text{Tf}_2\text{N}]$). They have shown that fine-grained and smoother deposits were obtained from the electrolytes with additives as compared to that without the additives.

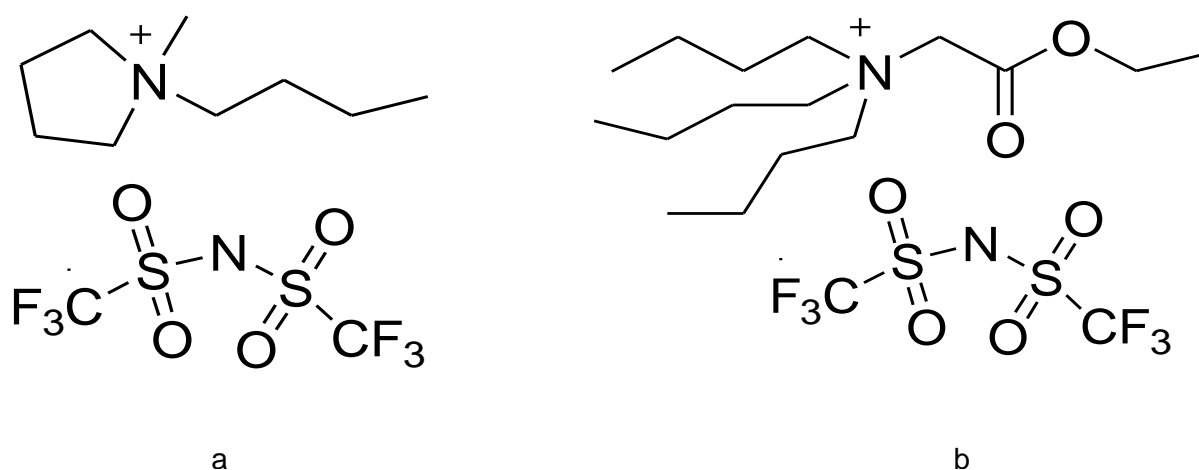


Figure 1. Chemical structure of ionic liquids used. (a) $[\text{BuGBOEt}][\text{Tf}_2\text{N}]$ and (b) $[\text{P}_{1,4}][\text{Tf}_2\text{N}]$.

The electrochemical behavior of divalent iron species with complexing agents have been reported by Yamagata et al. [27-28]. Some papers present the synthesis of Ni-Fe nanoparticles [29-30], nanowires [31] and thin films [32].

In this paper, we investigate the possibility to electroplate Fe, Ni and Ni-Fe alloys without hydrogen co-reduction using two ionic liquids at room temperature (Fig. 1). A study of the electrochemical behavior, structure, morphology and composition of thin films is presented.

2. EXPERIMENTAL

The electrodeposition of iron, nickel and nickel-iron was investigated in two different ionic liquid solvents. The first tested is the 1-butyl-1-methylpyrrolidinium bis(trifluoromethylsulfonyl)imide ([P_{1,4}][Tf₂N]). It came from Solvionic manufacturing (France) and was certified as high purity level (99.9 %). The second is the tri(*n*-butyl)[2-ethoxy-2-oxoethyl]ammonium bis(trifluoromethylsulfonyl)imide ([BuGBOEt][Tf₂N]). It is a homemade one.

2.1. Synthesis of tri(*n*-butyl)[2-ethoxy-2-oxoethyl]ammonium bis(trifluoromethylsulfonyl)imide ([BuGBOEt][Tf₂N])

For its preparation, tri(*n*-butyl)amine, ethyl 2-bromoacetate and lithium bis(trifluoromethylsulfonyl)imide bought from Sigma-Aldrich were used as received. The purity of resulted solvent was determined by elemental analyses carried out with Perkin-Elmer 2400 C, H, N element analyzer. ¹H NMR spectrum was recorded in DMSO-d₆ at room temperature with Brüker AC 250 spectrometer. Chemical shifts (in ppm) for ¹H NMR spectra were referenced to residual protic solvent peaks. The water contents in the ionic liquids were determined by Karl Fischer coulometry using Metrohm 787 KF Titrino coulometer. The Karl Fischer titrant was a two-component, Hydranal 34805 and Hydranal 37817, reagents provided by Fluka.

The synthesis of the hydrophobic ionic liquid was performed through two steps [33]. The cationic esters, derivatives of betaine tri(*n*-butyl)[(2-ethoxy-2-oxoethyl)ammonium bromide ([BuGBOEt][Br]) was successfully synthesized by the reaction of tri(*n*-butyl)amine and ethyl 2-bromoacetate.

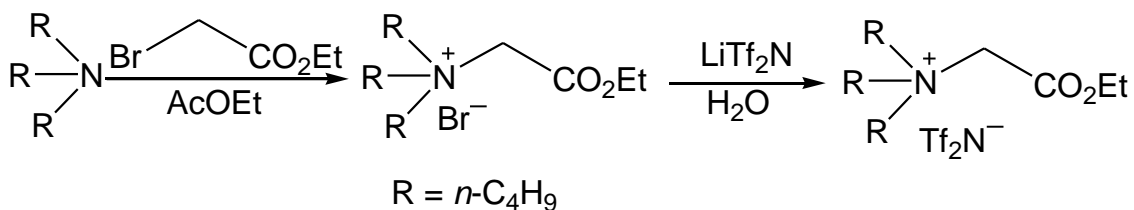


Figure 2. Synthetic route of the [BuGBOEt][Tf₂N].

The anionic metathesis of [BuGBOEt][Br] and LiTf₂N generates hydrophobic ionic liquid [BuGBOEt][Tf₂N] in quantitative yield (Fig. 2).

2.1.1. Tri(*n*-butyl)[2-ethoxy-2-oxoethyl]ammonium bromide ([BuGBOEt][Br])

To a solution of tri(*n*-butyl)amine (102 g, 0.55 mol) in ethyl acetate (150 mL) cooled down to 4 °C was added dropwise ethyl 2-bromoacetate (37.5 g, 0.22 mol). The mixture was then stirred at room temperature for 1 day. Precipitate produced during the reaction was filtered and washed with ethyl acetate. Recrystallization of the residue by ethanol/ethyl acetate (10:90, V:V) gave a white powder which was filtered, washed with ethyl acetate and dried *in vacuo*. Yield (65.9 g, 85 %). Melting Point 74 °C. Elemental analysis: Found: C, 54.52; H, 9.75; N, 3.98 %. Calculated for C₁₆H₃₄BrNO₂: C, 54.54; H, 9.73; N, 3.98%. ¹H NMR (250 MHz, DMSO-*d*₆): 0.93 (t, 9 H, -CH₃), 1.25 (t, 3 H, -CH₃), 1.30 (m, 6 H, -CH₂), 1.62 (m, 6 H, -CH₂), 3.43 (m, 6 H, -CH₂), 4.23 (s, 2 H, N-CH₂), 4.38 (q, 2H, O-CH₂).

2.1.2. Tri(*n*-butyl)[2-ethoxy-2-oxoethyl]ammonium bis(trifluoromethylsulfonyl)imide ([BuGBOEt][Tf₂N])

0.148 mol of [BuGBOEt][Br] was dissolved in water (100 mL) and a solution of Li[Tf₂N] (54.6 g, 0.22 mol) in water (100 mL) was added. The mixture was stirred for 3 hours, and then allowed to settle into two phases. The lower ionic liquid phase was extracted by ethyl acetate (50 mL) and washed with water (3 × 50 mL). The absence of bromide ions was controlled by an AgNO₃ test of the aqueous phase. The organic phase was dried over anhydrous MgSO₄, filtered, and the organic solvent was then evaporated under reduced pressure at 50 °C to give the product as a yellowish liquid (up to 85% conversion based on the cation). Elemental analysis exhibits a high purity of ionic liquid elaborated: Found: C, 39.28; H, 6.02; N, 5.03; S, 11.63%. Calculated for C₁₈H₃₄F₆N₂O₆S₄: C, 39.13; H, 6.20; N, 5.07; S, 11.60%. ¹H NMR (250 MHz, DMSO-*d*₆): 1.16 (t, 9H, -CH₃), 1.15 (t, 3H, -CH₃), 1.48 (t, 3H, -CH₃), 1.55 (m, 6H, CH₂), 1.86 (m, 2H, CH₂), 3.66 (m, 6H, O-CH₂), 4.59 (s, 2H, N-CH₂). H₂O, 0.24% (w/w).

2.2. Electrolytic conditions

For electrolyte preparation, ferrous perchlorate Fe(ClO₄)₂·6H₂O (purity ≥99.999%, Fluka) was chosen to introduce the iron metallic salt. For Ni dissolution, we could not have found any soluble salts in our solvents, so Ni(II) was introduced to the solution by dissolution of Ni(Tf₂N)₂ (purity ≥99.5%, Solvionic). All the metallic salts used have the concentrations of 0.1 mol.L⁻¹.

After dissolution of the metallic salts, and before the experimental stage, each solution was dried under vacuum at 80°C during 1 week in a manner to eliminate all water traces from solvent or from iron salt.

The electrochemical experiments were carried out at 50°C inside an argon-filled glove box with water and oxygen content below 1 ppm. In order to enhance the cell temperature, the electrochemical set-up was placed inside a homemade oven located inside the glove box. A conventional three-electrode set-up was used to perform experiments. All these electrodes were immersed in a unique compartment of a glass cell. A Teflon O-ring was used to delimitate the exposed surface (0.2 cm²) of the working electrode (WE). Copper disks were used as WE. Before electrodeposition, the copper

substrates were mechanically polished with silicon carbide paper and rinsed with 99.9% alcohol before drying. Platinum wire was used as counter electrode (CE). Before each experiment, the platinum wire was heated by flame for few seconds until glowing. For size reasons inside the oven, a wire was used as reference electrode (RE) which was treated by the same way as the working electrode. Two different materials (nickel and platinum) were tested. The choice of the quasi-references electrodes was decided after recording several time the intensity-potential curves and measuring the solvent reduction potential. The best stability was obtained with nickel wire (inferior to 35 mV versus more 100 mV with platinum wire). In consequence, all values of the potentials are reported with respect to the Ni quasi-reference electrode (noted /Ni in the discussion part).

The electrochemical measurements were conducted using Radiometer potentiostat-galvanostat PGZ 301 controlled by Voltmaster 4 software. All current density-potential curves were recorded only in the cathodic direction with scan rate of $2 \text{ mV}\cdot\text{s}^{-1}$. This weak scan rate was chosen in order to obtain the most accurate comparison between reductions steps and deposits composition.

2.3. Characterization methods

The morphology and the chemical composition of samples were characterized by JEOL JSM 6460LA Scanning Electron Microscope (SEM) coupled with EDS JEOL 1300 microprobe (EDXS).

X-ray diffraction investigations have been carried out using Bruker D8 Advance X-ray diffractometer equipped with a copper anticathode ($\lambda \text{ Cu K}\alpha = 1.54056 \text{ \AA}$).

3. RESULTS AND DISCUSSION

3.1. Iron electrodeposits

The deposition of iron was tested in the two ionic liquids and the results of electrochemical studies are individually presented below (voltammograms were scanned directly on the copper substrate with scan rate equal to $2 \text{ mV}\cdot\text{s}^{-1}$).

3.1.1. Iron electrodeposition in the $[P_{1,4}][Tf_2N]$ ionic liquid

The current density-potential curve for iron in the $[P_{1,4}][Tf_2N]$ was carried out and the result is shown in Fig. 3. The evolution of the solvent is obtained at about -4 V/Ni .

The voltammogram is complex to interpret and presents several reduction steps named $C1_{Fe}$, $C2_{Fe}$, $C3_{Fe}$ and $C4_{Fe}$ followed by the solvent reduction (sol). For applied potentials corresponding to the three first steps ($C1_{Fe}$, $C2_{Fe}$ and $C3_{Fe}$), no visible metallic deposit was obtained. These reduction waves can be due to the presence of different steps with intermediate adsorbed species ($Fe(I)_{ads}$). Future investigations of mechanism will be necessary to clarify each of these waves. In contrary to the first steps, $C4_{Fe}$ give metallic iron. After one hour of polarization and at the beginning of the $C4_{Fe}$

reduction wave (- 3 V/Ni), traces of iron appears. With the increase of polarization (- 4 V/Ni), iron deposition becomes more and more important (Fig. 4) but only some small area are covered (Fig. 5). For Fig. 4, the intensity were normalized and a value equal to 100 was attributed to the copper K α ray (copper ray corresponding to the substrate). The relative importance of the Cu K α ray compare to the one of the Fe K α indicates a weak quantity of iron.

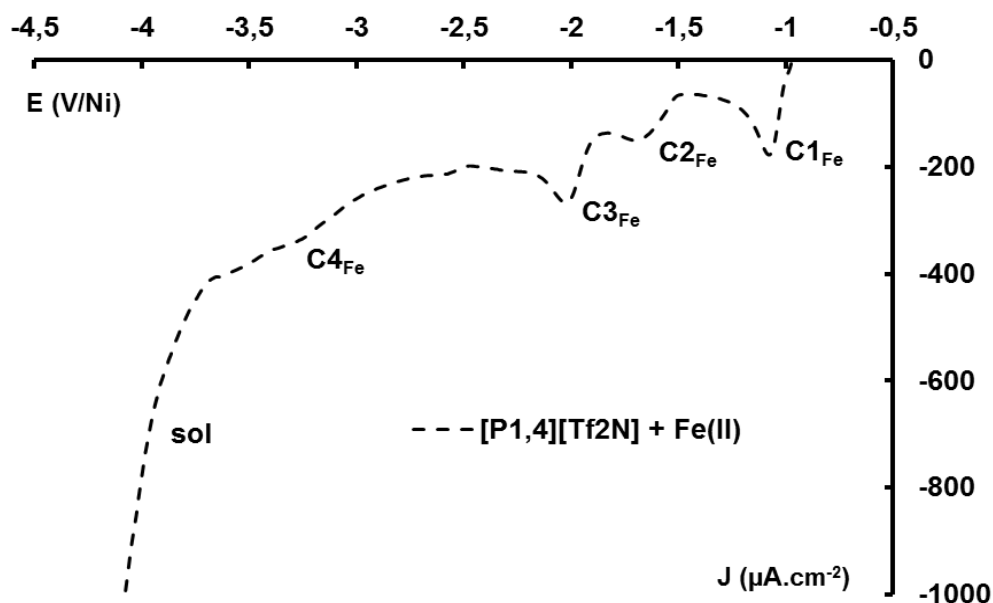


Figure 3. Current density-potential curve of [P_{1,4}][Tf₂N] containing 0.1 mol.L⁻¹ of Fe(II) at 50 °C on copper. Scan rate 2 mV.s⁻¹.

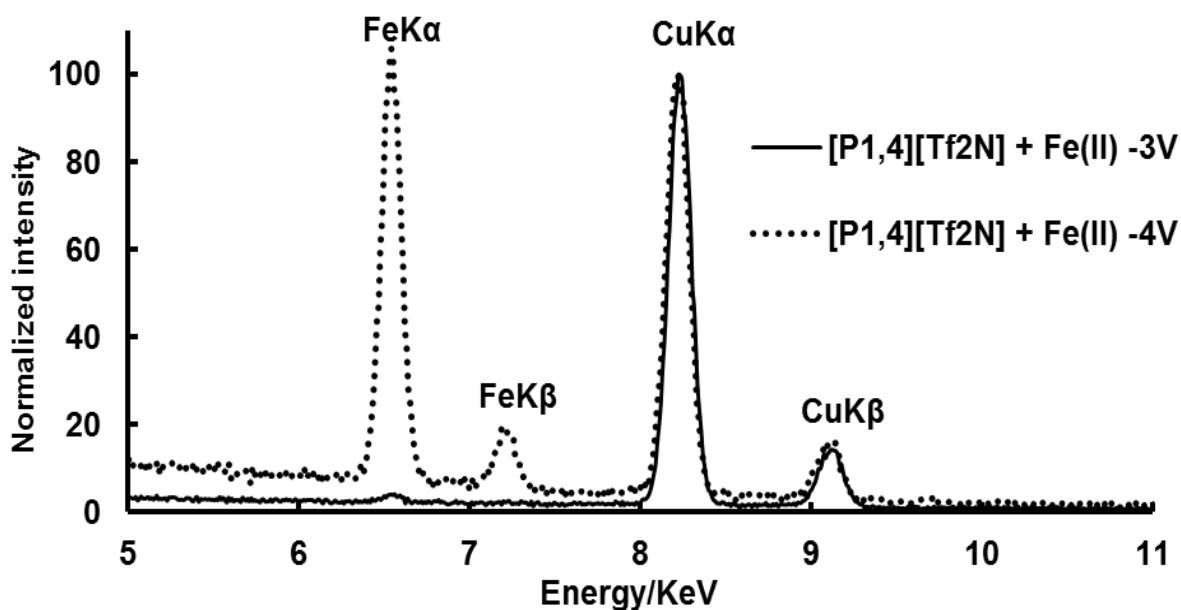


Figure 4. EDXS analysis of iron deposits obtained in [P_{1,4}][Tf₂N] containing 0.1 mol.L⁻¹ of Fe(II) at 50 °C on copper after 1 h of polarization. (a) - 3 V/Ni. (b) - 4 V/Ni.

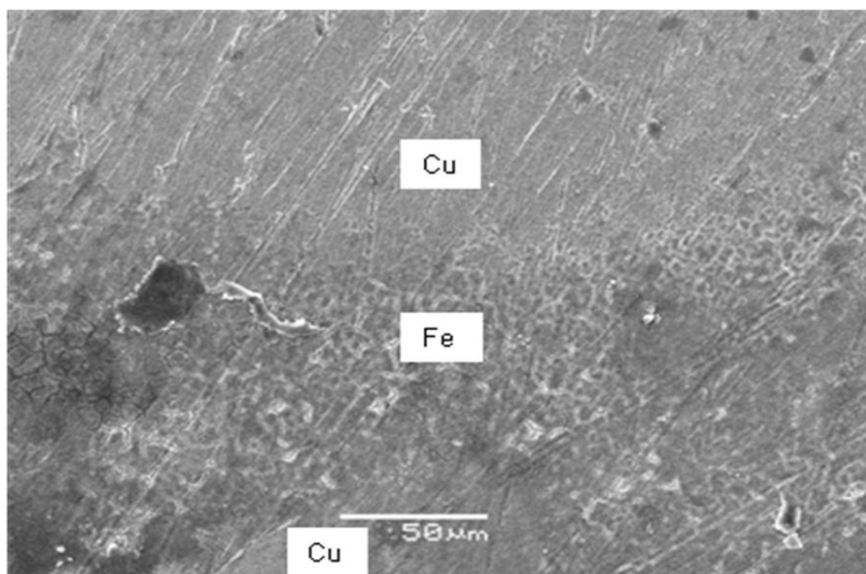


Figure 5. SEM micrograph of iron deposits obtained in $[P_{1,4}][Tf_2N]$ containing 0.1 mol.L^{-1} of $Fe(II)$ at $50 \text{ }^\circ\text{C}$ on copper after 1 h of polarization at -4 V/Ni .

3.1.2. Iron electrodeposition in the $[BuGBOEt][Tf_2N]$ ionic liquid

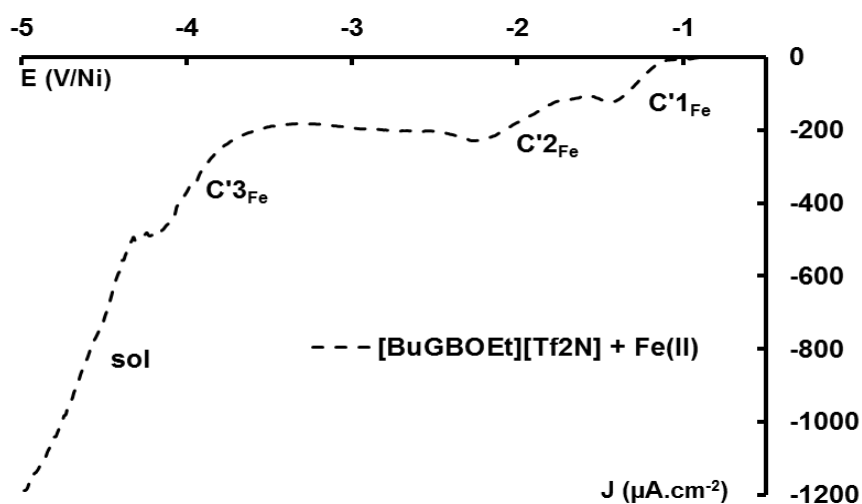
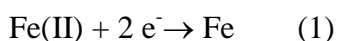


Figure 6. Current density-potential curve of $[BuGBOEt][Tf_2N]$ containing 0.1 mol.L^{-1} of $Fe(II)$ at $50 \text{ }^\circ\text{C}$ on copper. Scan rate 2 mV.s^{-1} .

Figure 6 exhibits the iron current density-potential curves obtained in the $[BuGBOEt][Tf_2N]$ solvent. Several cathodic steps, named $C'1_{Fe}$, $C'2_{Fe}$ and $C'3_{Fe}$ appear before the great evolution of the solvent at about -4.3 V/Ni . Contrary to the electrodeposition in the $[P_{1,4}][Tf_2N]$ ionic liquid, each wave leads to metallic deposits and could be attributed to the global equation (1).



The presence of iron metallic as soon as the first step and the presence of several reduction steps with limiting diffusion current means that Fe (II) ions are probably present in the solution under different complex forms. Some iron micrographs analyses are reported in Fig. 7. Whatever the polarization, deposits are totally covered but their morphology is affected by the applied potential.

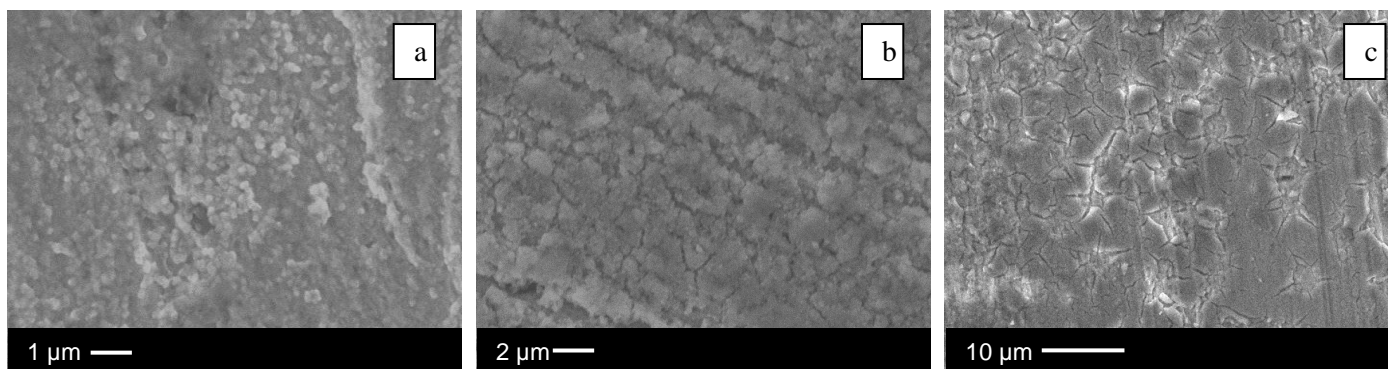


Figure 7. SEM micrographs of iron deposits obtained in [BuGBOEt][Tf₂N] containing 0.1 mol.L⁻¹ of Fe(II) at 50 °C on copper after 1 h of polarization. (a) - 1.4 V/Ni. (b) - 2.2 V/Ni. (c) - 3.8 V/Ni.

SEM micrograph presented in Fig. 7a (- 1.4 V/Ni) shows homogeneous iron deposits with small nodular shapes. For lower potentials (Fig. 7b and c), deposits become more and more compact with finer-grained surface. At - 3.8 V/Ni, the deposits present some cracks (Fig. 7c) which are certainly due to the internal stresses.

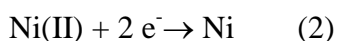
This new home-made solvent allows obtaining covered iron deposits without the classical inconvenient of hydrogen evolution observed in aqueous solvent while using Fe(ClO₄)₂ as metallic salt.

3.2. Nickel electrodeposits

For nickel electrodeposition, we only present the electrochemical results obtained with the 1-butyl-1-methylpyrrolidinium bis(trifluoromethylsulfonyl)imide ([P_{1,4}][Tf₂N]) ionic liquid. In fact, no classical nickel salts and no Ni(Tf₂N)₂ could be dissolved in the tri(n-butyl)[2-ethoxy-2oxoethyl]ammonium bis (trifluoromethylsulfonyl)imide ([BuGBOEt][Tf₂N]).

Figure 8 presents the current density-potential curves of nickel in the [P_{1,4}][Tf₂N]. As with iron voltamograms, the nickel reduction curve indicates several cathodic steps named C1_{Ni}, C2_{Ni}, C3_{Ni} and C4_{Ni} beginning respectively at - 1.7, - 2.2, - 3.0 and - 3.6 V/Ni. The solvent reduction (sol) is observed at about - 4 V/Ni.

Each cathodic step gives metallic deposits and could be attributed to the equation (2).



The presence of several reduction steps leading to nickel metallic as soon as the first one may have some explanations. Different complex forms of Ni(II) (with their own reduction potential) in solution and/or a modification of surface morphology (see Fig.9) can induce current evolution.

Note that Zhu *et al.* [32] have used the same solvent and the same nickel salt, but have only obtained a single reduction wave for nickel. This difference could be attributed to the scan rate to record their voltammograms ($2 \text{ mV}\cdot\text{s}^{-1}$ for us and $100 \text{ mV}\cdot\text{s}^{-1}$ for Zhu *et al.*). Indeed, at high scan rate, the slow kinetic reactions could be masked [34] and the evolutions of surface have not time to take place.

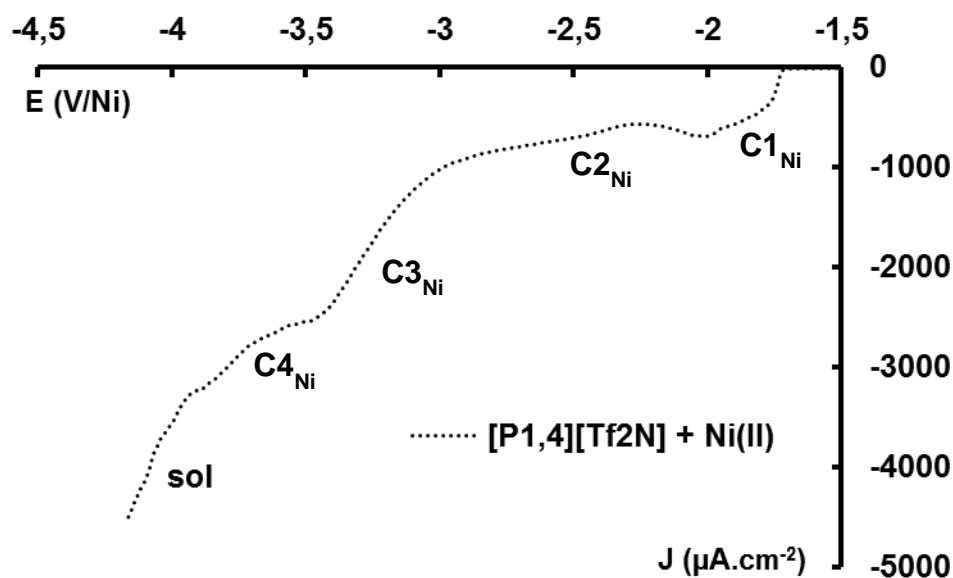


Figure 8. Current density-potential curve of $[\text{P}_{1,4}][\text{Tf}_2\text{N}]$ containing $0.1 \text{ mol}\cdot\text{L}^{-1}$ of $\text{Ni}(\text{II})$ at $50 \text{ }^\circ\text{C}$ on copper. Scan rate $2 \text{ mV}\cdot\text{s}^{-1}$.

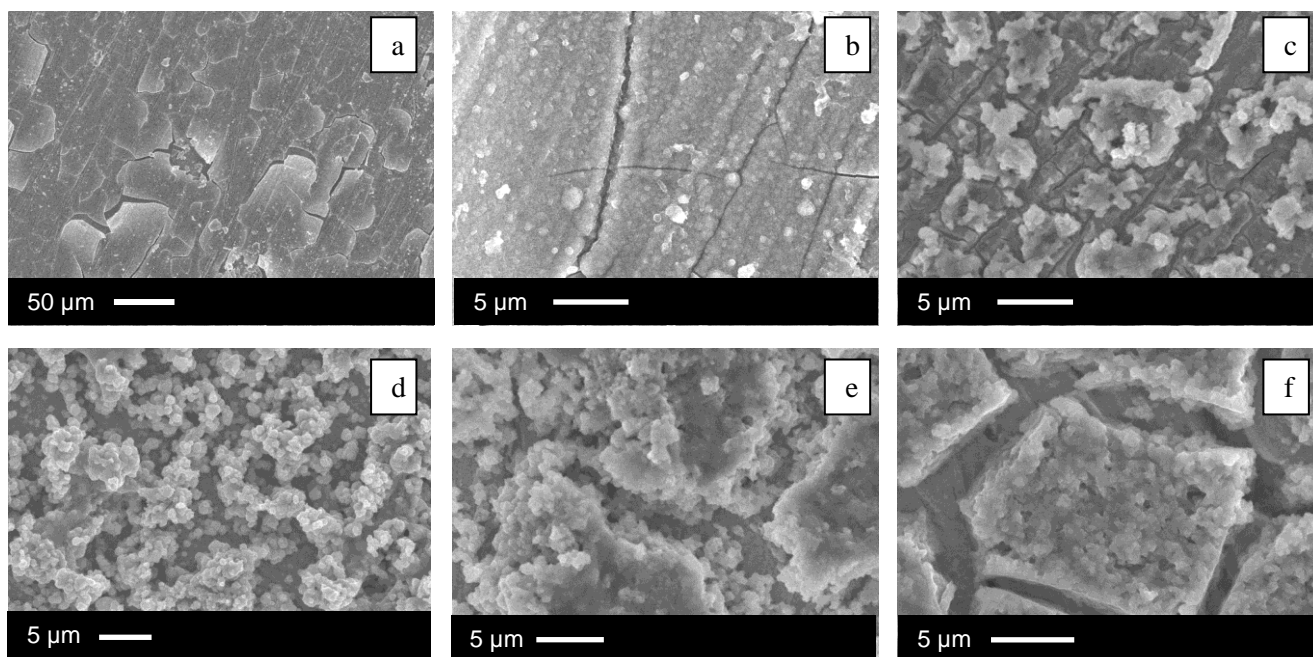


Figure 9. SEM micrographs of nickel deposits obtained in $[\text{P}_{1,4}][\text{Tf}_2\text{N}]$ containing $0.1 \text{ mol}\cdot\text{L}^{-1}$ of $\text{Ni}(\text{II})$ at $50 \text{ }^\circ\text{C}$ on copper after 1 h of polarization. (a) and (b) - 2.25 V/Ni . (c) - 2.5 V/Ni . (d) - 3 V/Ni . (e) - 3.75 V/Ni . (f) - 4 V/Ni .

Some SEM micrographs of nickel coatings are presented in Fig. 9. The deposits were composed of many fragments for the most positive potential (Fig. 9a and b). The surface of each fragment seems to be relatively smooth with undefined grains. However, the deposits of nickel were transformed from smooth cracks to three-dimensional clusters of Ni grains when the applied potentials were more negative (Fig. 9c). These nickel clusters sharply increase from the surface to the underlying cracks (Fig. 9d). This significant change in the surface morphology corresponds respectively to the apparition of the steps C_{2Ni} and C_{3Ni} (Fig. 8). When the polarization increases again, the observed cracks seem to be more and more filled with the aggregations of large grains (Fig. 9e) corresponding to the beginning of the C_{4Ni} wave. At potentials more negative (Fig. 9f) this phenomenon seems to be stopped. The surface morphology shows fragments with the presence of clusters of less rough structure.

3.3. Ni-Fe alloys electrodeposits

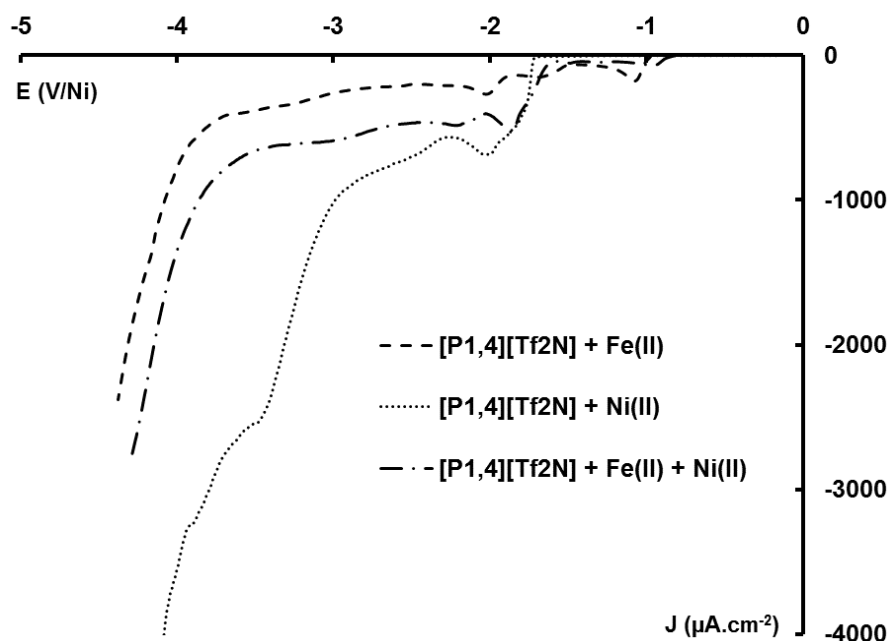


Figure 10. Current density-potential curves of $[P_{1,4}][Tf_2N]$ at 50 °C on copper. Scan rate $2 \text{ mV}\cdot\text{s}^{-1}$
¹Dashed curve: $[P_{1,4}][Tf_2N]$ containing $0.1 \text{ mol}\cdot\text{L}^{-1}$ of Fe(II), dotted curve: $[P_{1,4}][Tf_2N]$ containing $0.1 \text{ mol}\cdot\text{L}^{-1}$ of Ni(II), alternating dashed-dotted curve: $[P_{1,4}][Tf_2N]$ containing $0.1 \text{ mol}\cdot\text{L}^{-1}$ of Fe(II) and $0.1 \text{ mol}\cdot\text{L}^{-1}$ of Ni(II).

As tested nickel salts are not soluble in the $[BuGBOEt][Tf_2N]$ solvent, the electrodeposition of Ni-Fe alloys was conducted only in the $[P_{1,4}][Tf_2N]$ solvent. Fig. 10 displays the current density-potential curves recorded in the $([P_{1,4}][Tf_2N])$ solvent containing $0.1 \text{ mol}\cdot\text{L}^{-1}$ of $Fe(ClO_4)_2\cdot 6H_2O$ and $0.1 \text{ mol}\cdot\text{L}^{-1}$ of $Ni(Tf_2N)_2$ (alternating dash-dotted). This curve was overlaid with that of iron (dashed curve) and nickel (dotted curve) in $([P_{1,4}][Tf_2N])$. For each curve the scan rate was equal to $2 \text{ mV}\cdot\text{s}^{-1}$. The comparison between these different curves requests several comments. Firstly, when Ni is the only

electroactive specie, the cathodic current is more important than that obtained for only Fe specie. This phenomenon is, in part, due to the active surface morphology. Indeed, the active surface of Ni thin film (Fig. 9) is more important (covered surface with many nodules) than that of Fe (no covered surface) (Fig. 5). Secondly, the values of the cathodic current density-potential curve are lower for Ni(II)-Fe(II) solution than that obtained for Ni(II) solution, probably due to a lower active surface. Figure 11 exhibits SEM micrographs of deposits obtained for different overpotentials. Two different forms of crystals are observed: circular shapes (Fig. 11a and c) and nodular forms (Fig. 11b).

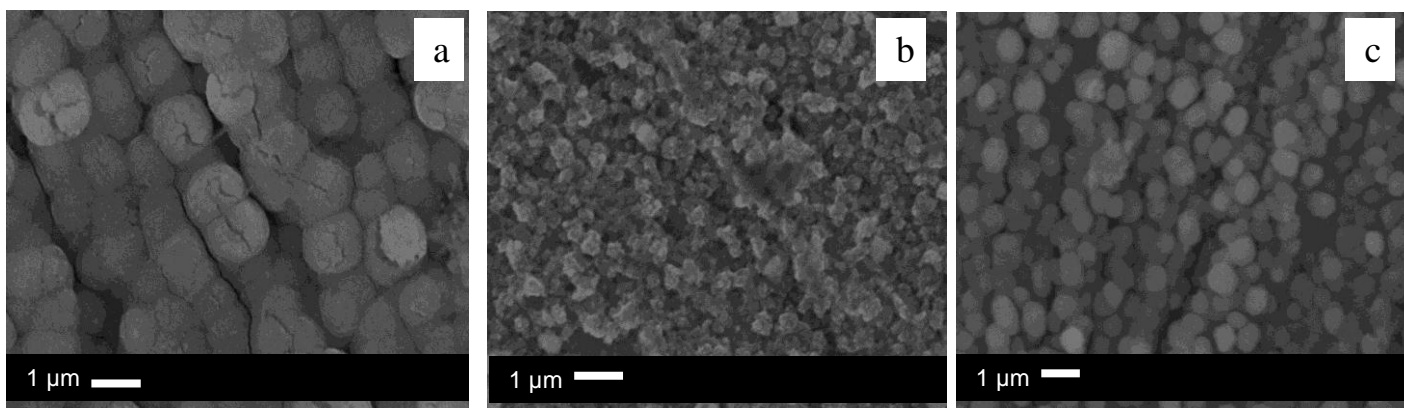


Figure 11. SEM micrographs of nickel-iron alloys deposits obtained in $[P_{1,4}][Tf_2N]$ containing 0.1 mol.L^{-1} of Fe(II) and 0.1 mol.L^{-1} of Ni(II) at $50 \text{ }^\circ\text{C}$ on copper after 1 h of polarization. (a) - 2.15 V/Ni . (b) - 2.5 V/Ni . (c) - 3.75 V/Ni .

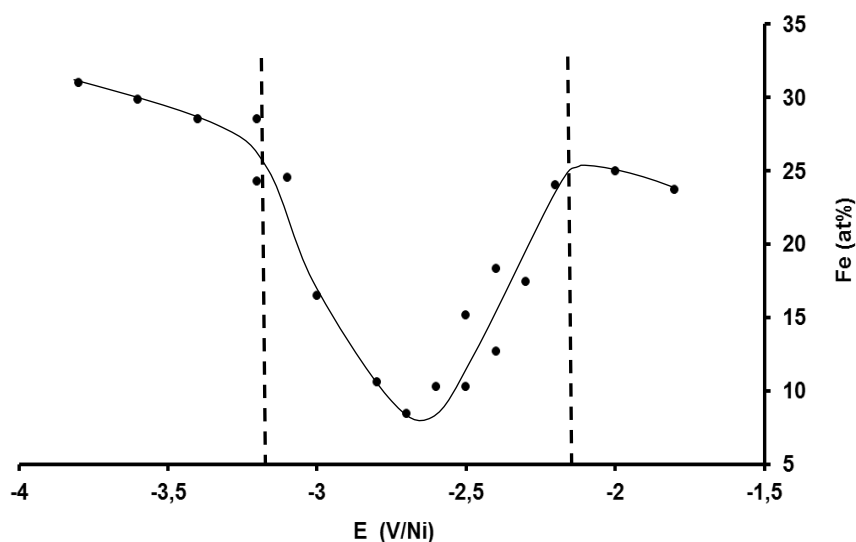


Figure 12. Evolution of iron atomic percentage in the nickel-iron alloys versus applied potential obtained in $[P_{1,4}][Tf_2N]$ containing 0.1 mol.L^{-1} of Fe(II) and 0.1 mol.L^{-1} of Ni(II) at $50 \text{ }^\circ\text{C}$ on copper after 1h of polarization.

Figure 12 shows the evolution of iron atomic percentage inside the plated Ni-Fe alloys versus applied potential. It is interesting to note that even if we have not obtain covering Fe deposit with this solvent, Ni-Fe alloys with respectable iron atomic percentage become possible. Note also, the strange evolution of the composition that does not correspond to a regular progression versus overpotential (firstly, an increase in the iron atomic percentage versus overpotential, followed by a surprising decrease of iron quantity and finally by a new increase of iron percentage). This phenomenon is related to the presence of different stages in the Ni-Fe density-potential curve. The potential range of the iron atomic percentage fall is obtained between about - 2.15 V/Ni and - 3.15 V/Ni. It is interesting to correlate this zone with the modification of morphology observed in Fig. 11 between circular shapes (Fig. 11a and c) and nodular shapes (Fig. 11b). Note that the value of the beginning of the fall corresponds to the beginning of the C2_{Ni} step (Fig. 8). Adsorption competition between Ni and Fe could be responsible of this phenomenon.

Finally, note that iron percentage in all electrodeposited alloys is lower than the ratio of individual Ni and Fe in the bath. Opposite results (Fe atm.% > Ni atm.%) are obtained in aqueous solution [11] due to the anomalous co-deposition [1]. The fact that the Ni atm.% is higher in the studied solvent was already observed by Zhu *et al.* [32]. They explained that by a non-anomalous co-deposition in the [P_{1,4}][Tf₂N].

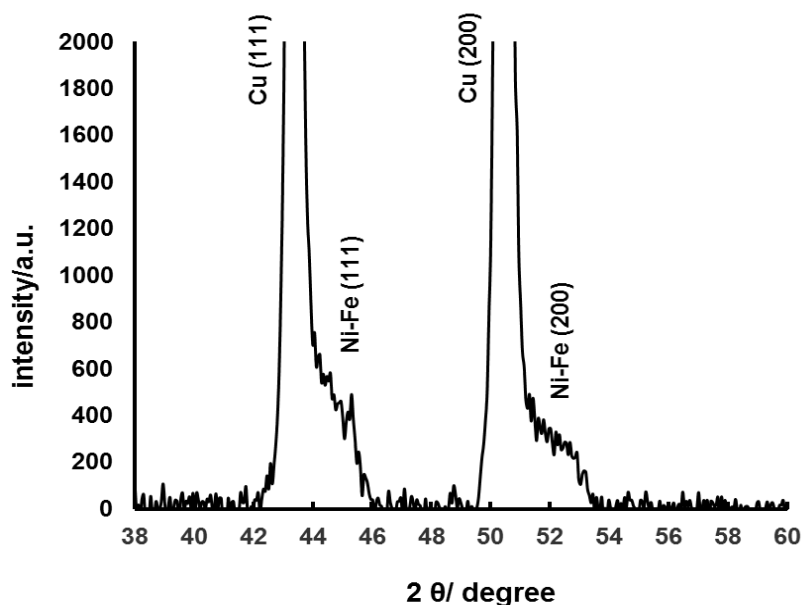


Figure 13. XRD patterns of nickel-iron alloys obtained at - 3.5 V in [P_{1,4}][Tf₂N] containing 0.1 mol.L⁻¹ of Fe(II) and 0.1 mol.L⁻¹ of Ni(II) at 50 °C on copper after 1 h of polarization.

The samples were also analyzed by X-ray diffraction. An example is reported in Fig.13. Two peaks corresponding to the Cu (111) and Cu (200) from substrate respectively at 43.3° and 50.4 ° and

two no well-defined peaks assignable to the Ni-Fe (111) and Ni-Fe (200) alloys are observed. Similar results were obtained by Zhu *et al.* [32] for Ni-Fe alloys electrodeposited with weak charge density.

4. CONCLUSION

This study shows the possibility to plate Fe, Ni and Ni-Fe in ionic liquids solvents without hydrogen evolution.

For the first time the tri(*n*-butyl)[2-ethoxy-2oxoethyl]ammonium bis(trifluoromethylsulfonyl)imide ([BuGBOEt][Tf₂N]) was tested for electrodeposition. Results are very encouraging because this solvent allows electroplating iron thin films. Note that iron deposits have not been obtained for potential values superior to - 3 V/Ni using the 1-butyl-1-methylpyrrolidinium bis(trifluoromethylsulfonyl)imide ([P_{1,4}][Tf₂N]). In this study, nickel electrodeposition was only possible in the [P_{1,4}][Tf₂N]. It is important to remark that Ni-Fe alloys electrodeposition was obtained with success in [P_{1,4}][Tf₂N] even if iron films is difficult to plate alone. Finally, a surprising evolution of the alloy composition versus polarization (increase, decrease and increase of iron atomic percentage) was observed.

References

1. A. Brenner, *Electrodeposition of alloys*, Academic Press Inc, New York, 1963.
2. E. Kondorsky, I. Sedov, *V. L. J. Appl. Phys.*, 31 (1960) S331.
3. P. Andricacos, P.C. Arana, C. Tabib, J. Dukovic, J. Romankiw, *L.T.J. Electrochem. Soc.*, 136 (1989) 1336.
4. R. Karthik, R. J. Raja, M. Ramasamy, G. Sheela, S. Madhu, S. Kennedy, C. H. Ramakishan Rao, M. Pushpavanam, *Trans. Inst. Met. Fin.* 81 (2003) 68.
5. D. L. Grimmitt, M. Schwartz, K. Nobe, *Plating and Surface Finishing*, 75 (1998) 94.
6. A. Ramachandran, C. N. Tharamani, S. M. Mayanna, *Trans. Inst. Met. Finish.* 79 (2001) 195.
7. F. Ebrahimi, Z.J. Ahmed, *App. Electrochem.*, 33 (2003) 733.
8. K. Msellak, J. P. Chopart, O. Jbara, O. Aaboubi, J. Amblard, *J. Magn. Magn. Mater.* 281 (2004) 295.
9. I. Tabakovic, S. Riemer, V. Vas'Ko, V. Sapozhnikov, M. Kief, *J. Electrochem. Soc.*, 150 (2003) C635.
10. C. Rouse, K. Msellak, P. Fricoteaux, E. Merienne, J. P. Chopart, *Magneto hydrodynamics.*, 42 (2006) 371.
11. P. Fricoteaux, C. Rouse, *J. Electroanal. Chem.*, 612 (2008) 9.
12. C. Rouse, P. Fricoteaux, *J. Mater. Sci.*, 46 (2011) 6046.
13. P. Wasserscheid, T. Welton, *Ionic Liquids in Synthesis*, Wiley-VCH, VerlagGmpH 2003.
14. F. Endres, S. Zein El Abedin, *Phys. Chem. Chem. Phys.*, 8 (2006) 2101.
15. F. Endres, A. P. Abbott, D. R. MacFarlane, *Electrodeposition from Ionic Liquids*, Wiley-VCH, Weinheim 2008.
16. T. P. Moffat, *J. Electrochem. Soc.*, 141 (1994) 3059.
17. W. R. Pitner, C. L. Hussey, G. R. Stafford, *J. Electrochem. Soc.*, 143 (1996) 130.
18. C. A. Zell, W. Freyland, *Chem. Phys. Lett.*, 337 (2001) 293.
19. S. P. Gou, I. W. Sun, *Electrochim. Acta.*, 53 (2008) 2538.

20. F. Endres, *Chem. Phys. Chem.*, 3 (2002) 144.
21. S. I. Hsiu, I. W. Sun, *J. Appl. Electrochem.*, 34 (2004) 1057.
22. F. Endres, S. Zein El Abedin, *Chem. Commun.*, 2002, 892.
23. A. P. Abbott, K. J. MacKenzie, *Phys. Chem. Chem. Phys.*, 8 (2006) 4265.
24. H. Ohno, *Electrochemical Aspects of Ionic Liquids*, John Wiley & Sons, New York 2005.
25. Y. L. Zhu, Y. Katayama, T. Miura, *Electrochim. Acta.*, 55 (2010) 9019.
26. Y. L. Zhu, Y. Katayama, T. Miura, *Electrochim. Acta.*, 85 (2012) 622.
27. M. Yamagata, N. Tachikawa, Y. Katayama, T. Miura, *Electrochemistry*, 73 (2005) 564.
28. M. Yamagata, N. Tachikawa, Y. Katayama, T. Miura, *Electrochim. Acta.*, 52 (2007) 3317.
29. Y. L. Zhu, Y. Katayama, T. Miura, *ECS Transactions*, 33 (2010) 537.
30. Y. L. Zhu, Y. Katayama, T. Miura, *Electrochemical and Solid State Letters*, 14 (2011) D110.
31. X. Zhang, H. Zhang, T. Wu, Z. Li, Z. Zhang, H. Sun, *J. Magn. Magn. Mater.*, 331 (2013) 162.
32. Y.L. Zhu, Y. Katayama, T. Miura, *J. Electrochem. Soc.*, 162 (2015) D371.
33. A. Messadi, A. Mohamadou, S. Boudesocque, L. Dupont, P. Fricoteaux, A. Nguyen-Van-Nhien, M. Courty, *J. Mol. Liquids*, 184 (2013) 68.
34. C. Rousse, S. Beaufils, P. Fricoteaux, *Electrochim. Acta.*, 107 (2013) 624.

© 2016 The Authors. Published by ESG (www.electrochemsci.org). This article is an open access article distributed under the terms and conditions of the Creative Commons Attribution license (<http://creativecommons.org/licenses/by/4.0/>).